



UvA-DARE (Digital Academic Repository)

Building tools for image-guided adaptive radiotherapy of bladder cancer

Chai, X.

Publication date
2012

[Link to publication](#)

Citation for published version (APA):

Chai, X. (2012). *Building tools for image-guided adaptive radiotherapy of bladder cancer*. [Thesis, fully internal, Universiteit van Amsterdam]. Boxpress.

General rights

It is not permitted to download or to forward/distribute the text or part of it without the consent of the author(s) and/or copyright holder(s), other than for strictly personal, individual use, unless the work is under an open content license (like Creative Commons).

Disclaimer/Complaints regulations

If you believe that digital publication of certain material infringes any of your rights or (privacy) interests, please let the Library know, stating your reasons. In case of a legitimate complaint, the Library will make the material inaccessible and/or remove it from the website. Please Ask the Library: <https://uba.uva.nl/en/contact>, or a letter to: Library of the University of Amsterdam, Secretariat, P.O. Box 19185, 1000 GD Amsterdam, The Netherlands. You will be contacted as soon as possible.

Chapter 3

Finite element based bladder modeling for image-guided radiotherapy of bladder cancer

Xiangfei Chai, Marcel van Herk, Jeroen B. van de Kamer, Maarten C.C.M. Hulshof,
Peter Remeijer, Heidi T. Lotz and Arjan Bel

Medical Physics, 2011 Jan; 38(1);142-50

Abstract:

Purpose: A biomechanical model was constructed to give insight into pelvic organ motion as a result of bladder filling changes.

Methods: We used finite element (FE) modeling to simulate bladder wall deformation caused by urine inflow. For 10 volunteers, a series of MRI scans of the pelvic area was recorded at regular intervals of 10 min over 1 hour. For the series of scans, the bladder volume gradually increased while rectal volume was constant. The MR image with bladder volume closest to 250 ml was selected as reference in each volunteer. All pelvic structures were defined from the reference image including bladder wall, small bowel, prostate (male), uterus (female), rectum, pelvic bone and the rest of the body. These structures were translated to FE meshes. Using appropriate material properties for all organs, deformations of these organs as a response to changing bladder pressure were computed.

Results: The computation results showed realistic anisotropic deformation of bladder wall: the bladder became more elongated in the cranial and anterior directions with increasing bladder volume. After fitting the volume of the computed bladder to the actual bladder volume on the test images, the computed bladder shape agreed well with the real bladder shape (overlap from 0.79 to 0.93). The average mean bladder wall prediction errors of all the volunteers were 0.31 cm average and 0.29 cm SD.

Conclusions: In conclusion, a FE based mechanical bladder model shows promise for the prediction of the short term bladder shape change only using one pelvic scan and volume change of the bladder as input. The accuracy levels achieved with this method are likely mostly limited by inaccuracies in material properties and sliding tissue between organs, which has not been modeled. This model can potentially be used to improve image-guided radiotherapy for bladder cancer patients, i.e., by prediction short-term bladder deformation.

3.1 Introduction

Modern radiotherapy techniques allow for planning and delivery of complex dose distributions, which enable an increase in the dose to target volumes and a better sparing of normal tissue. However, anatomical changes in patients limit the benefits of these techniques. For example, organ deformation between fractions of dose delivery [70] and motion during radiation dose delivery [71] can both potentially cause underdosage of the target volumes and overdosage of organs at risk.

It is well-known that for radiotherapy of pelvic tumors, the bladder filling is a typical cause of inter- and intra-fractional movement. For instance, uncertainty in location of bladder tumors can be as much as 3 cm, because of changes in volume of bladder and adjacent organs, such as small bowel, sigmoid colon, rectum, uterus, prostate and seminal vesicles [15;18;36]. Besides the day-to-day bladder wall movement, significant intra-fraction bladder wall displacement may occur during bladder RT delivery [37;72]. Bladder volume change is a main driving force causing cervix uteri deformation, and a few studies found that deformation of uterus can be partially explained by variations in bladder volume [73-75]. Bladder volume changes have also been reported to alter the position of prostate [76-78]. Numerous groups [15;76-79] give patients drinking instructions to standardize bladder volume, however, the effect is limited and the guidelines do not result in consistent bladder filling.

For bladder cancer, fiducial marker techniques have been introduced to mark the border of bladder tumor and movement of bladder tumor can be successfully tracked by using online cone beam CT (CBCT) [33;80;81]. However, the deformable bladder wall is often poorly visible in daily CBCT image because of the poor soft-tissue contrast. Thus, the dose on the healthy part of the bladder cannot be accurately determined. Short term bladder deformation between CBCT acquisition and dose delivery leads to geometrical uncertainties in bladder cancer treatment. Hence, to meet these two challenges, it is essential to study the mechanics of the bladder deformation process to allow improving the precision of the treatment.

Lotz et al. [40;82] used a linear model to describe the bladder shape and position as a function of the bladder volume and the rectal filling. Sohn et al. [83] modeled individual geometric variation of prostate, rectum and bladder by principal component analysis. Patient-specific geometric variation observed in multiple imaging data can be described accurately by a few dominating eigenmodes. These two models found that the bladder deformation pattern is patient dependent and therefore several prior images are required to build a patient-specific geometric model.

From a mechanical point of view, most pelvic organs are deformable bodies. Due to the external and internal organ loadings, such as inlet of urine, the organs move and interact with each other, under kinematic constraints. The patient-specific deformation patterns found by Lotz et al. and Sohn et al. [82;83] could perhaps be explained by a mechanical model where different patients have specific geometries and material properties.

The finite element (FE) method is a numerical technique where a mechanical model is built by solving partial differential equations. Recently, FE has been used to simulate the mechanical deformation of soft tissue during surgery [84] and medical

examinations [85]. However, only limited investigations have been performed for the simulation of anatomical variation that are relevant for radiotherapy [86-88].

In this work, we used a 3D FE method to model the specific geometry and simulate the interaction between the bladder and adjacent pelvic structures. This approach can potentially predict the movement of the bladder and its surrounding organs, based on a single geometric model (i.e., derived from a planning CT), using just bladder volume as input. The aim of this paper is to introduce this approach and test the accuracy of the model to predict short term bladder deformation.

3.2 Materials and methods

3.2.1 Data acquisition

Coronal MRI datasets were acquired from 10 healthy volunteers (5 males and 5 females). The median age of the volunteers was 43 years (range: 26-63). Volunteers were instructed to empty their bladder and drink 300 ml water 15 min prior to acquisition. The volunteers were positioned supine without immobilization and a pelvic phased array coil was applied. For each volunteer, a series of MRI scans of the pelvic area was recorded at regular intervals of 10 min over a period of one hour. Imaging was done with on a 1.5 T system (Somatom: Siemens Medical Systems, Erlangen, Germany). The following MRI parameters were used: T2-weighted sequence, repetition times: 8.1 ms, echo time: 4.0 ms, reconstruction in-plane matrix: 256*256 pixels, isotropic in-plane resolution: 1.4*1.4 mm², and section thickness: 1.4 mm.

The dataset in this work is the same as was used in a previous paper [40].

3.2.2 Biomechanical model of tissue deformation

As elastic materials, human tissue motion must obey the laws of mechanics. Geometrical motion of the organ due to respiration, internal fluid distribution and surrounding tissue traction can be described by using constitutive equations based on mechanical and mathematical laws [89].

Tissue deformation can be characterized as a minimum variation of total energy described as:

$$\Delta = \frac{1}{2} \int_{\Omega} \sigma^T \varepsilon d\Omega + \int_{\Omega} F^T D d\Omega \quad (3.1)$$

where Ω represents the continuous domain of an elastic body, F is the external force, D is the displacement in domain Ω and σ is the stress vector and ε is the strain vector. In three-dimensional continuum mechanics, a strain tensor written as $\varepsilon = [\varepsilon_x, \varepsilon_y, \varepsilon_z, \gamma_{xy}, \gamma_{yz}, \gamma_{xz}]^T$ is related to stress σ through Hooke's law, i.e. $\sigma = [C] \varepsilon$, where the matrix C is defined by the elasticity matrix characterizing the material's properties. Finally, the

strain is related to displacement by the assumption that $\varepsilon = L^T D$, where L is a linear differential operator [90].

Using an FEM approach, the problem domain Ω can be divided into discrete elements, with each element consisting of several nodes. The element type is assumed to be tetrahedral. The displacements of the points inside the element are obtained through the interpolation of node displacements, i.e. for each point x in the element e , $D(x) = \sum_{i=1}^4 N_i^e(x) D_i$ where $N_i^e(x)$ are the basis functions over the element e [91]. The unknown displacements D_i of these nodes are subjected to imposed force, elastic model and boundary constraints, which are usually calculated by solving a set of algebraic equations.

The minimization of the total energy in equation (3.1) using the variation principle, the relation between the vectors of displacements D and elastic forces F at each node i given the forces and acting on the boundary nodes is:

$$KD = -F \quad (3.2)$$

The displacements on the boundary nodes are fixed to match those generated by the surface correspondence estimates. This is done by setting all elements on rows K corresponding to boundary elements to zero, except for the diagonal that is set to 1. The corresponding right hand side element is set equal to the specified displacement value. Solving equation (3.2) for unknown displacements will produce a deformation field over entire mesh, and the prescribed displacements at boundary nodes will be preserved.

3.2.3 Finite element model construction

Generally, the FE method consists of the following three steps. First the problem domain is decomposed into a large number of elements which are connected via nodes located on their boundaries. Then, the load and boundary condition are defined. Finally, the displacement field in response of the load is calculated by solving partial differential equations (steps 4, 5 and 6 of figure 3.1). The other steps of figure 3.1 have to do with pre- and post-processing.

In each series of MR images, a single observer manually delineated the outer bladder wall on every image. In a previous study, 250 cm³ was found to be the average bladder volume in planning CT [81], so the image with a bladder volume closest to 250 cm³ was selected as reference. For the reference image, the other pelvic structures i.e. small bowel, prostate, rectum, pelvic bone, spine and body contour were also manually delineated (step 1 in figure 3.1). Since manual contouring of the inner bladder wall was difficult and not reliable on the T2 weighted MR image, the inner bladder contour was created by uniformly shrinking the outer bladder wall by 3 mm, which value was reported as the average bladder wall thickness by Hakenberg et al. [92]. All the contours on the reference image were used to build surface and volume meshes.

The contours on the reference image were converted to binary images and next converted into a triangular surface mesh using the marching cubes algorithm [93]. This algorithm created a triangle representation based on the intersection of the 3D contour surface with each voxel. The rough texture of the generated contour surface (figure 3.2 (a)) was different from real organ shape, so the jagged surface was eliminated by smoothing filter. The surface smoothing step generates more regular triangulations and improves the quality of volume meshes which are generated based on the triangulations.

The surface meshes were smoothed by iteratively moving each vertex to the average position of its neighboring vertices. After smoothing, the connectivity of mesh and number of vertices were unchanged, while the appearance and shape of the surface mesh were improved. For all the meshes, the smoothing was performed with 5 iterations, except for smoothing on the body contour which required 10 iterations. To obtain a reasonable volume mesh size, the number of triangles describing the surface was reduced. The surface meshes of the inner bladder, outer bladder, prostate, rectum and small bowel were reduced to 10% of original mesh size, while the surface meshes on spine, pelvic bone and body contour was reduced to 2 % of the original size. The number of vertices depends on the volume of organs. On average, the number of vertices on the bladder surface was 800. After mesh reduction, the surface was smoothed again by the same smoothing filter. An example of this pre-processing of the outer bladder is given in figure 3.2.

The smoothed triangular surface meshes representing the segmented organs were imported into a commercial FE method software package (Abaqus version 6.9 Dassault Systemes Simulia BV). Then subtraction (Boolean operation) between surface meshes was done to create the bladder wall and surrounding pelvic tissues other than pelvic organs. The surrounding tissue consisting of all anatomy not specifically delineated is referred to as “body”. Totally, seven organs were created which were bladder wall, small bowel, rectum, prostate (uterus for female), spine, pelvis and body. The seven organs were assembled as an entire model indicated in step 3 of figure 3.1. Then, surface interfaces and organ-specific material properties were assigned to each organ. A simple linear elastic material model was chosen with the parameters for each organ as shown in table 3.1. The linear material properties are characterized by two parameters: Young’s modulus E and Poisson’s ratio ν . A larger Young’s modulus indicates a stiffer material and a larger Poisson’s ratio indicates a less compressible tissue. The material properties were taken from literature [94;95], except for the small bowel and the uterus, which were considered as a bulk tissue. The material properties of uterus and small bowel were found by optimizing on a subset of the volunteers and applied to all test population. Using the starting values of $E = 10$ kPa and $\nu = 0.49$, trial simulations were made iteratively varying the values of E and ν of small bowel and uterus on three cases. By separately varying the values of material properties for these two organs, a set of values was obtained (small bowel: $E = 3$ kPa $\nu = 0.35$; uterus: $E = 20$ kPa and $\nu = 0.45$), when the model produced the most accurate results for bladder shape prediction.

Table 3.1: Applied linear elastic material parameters for pelvic organs.

| Organs | Poisson ratio (ν) | Young's modulus (E)(kPa) |
|-------------------------|-------------------------|------------------------------|
| Bladder | 0.49 | 10 |
| Pelvic tissue ("body") | 0.40 | 15 |
| Bone (spine and pelvis) | 0.49 | 1, 000 |
| Prostate (male) | 0.40 | 21 |
| Uterus (female) | 0.49 | 20 |
| Rectum | 0.45 | 10 |
| Small bowel | 0.35 | 3 |

Next, a 3D four-node tetrahedral volume mesh was next created from all surface meshes using the free meshing method in the Abaqus package, as shown in step 4 of figure 3.1. By setting the global element size to 2 mm, on average 200, 000 tetrahedral elements were generated for each model including all the organs. All elements belonging to the same organ were assigned the same material properties.

As bladder filling is a rather slow process, the bladder filling increase is considered as a static kinematic process. During the scan session, the rectal filling did not change significantly, as was reported in a previous study [40] and we also assumed the external forces applied on other pelvic organs had not changed. So, bladder filling was the only reason causing deformation of the pelvic region. An internal pressure of 1 kPa was uniformly applied on the inner bladder wall to simulate an arbitrary bladder filling increase. The exact bladder pressure corresponding to the know volume was unknown, however since this model was a linear system, the deformation caused by different pressure could be calculated by scaling the results until the desired volume was reached. During scanning, volunteers lay on the table in supine position with an MR coil attached to belly. Hence, the kinematic boundary conditions were such that the nodes on back position were fixed in all directions and the nodes on the abdomen were restrained from any displacement along anterior-posterior direction. Loads and boundary conditions are illustrated in step 5 of figure 3.1.

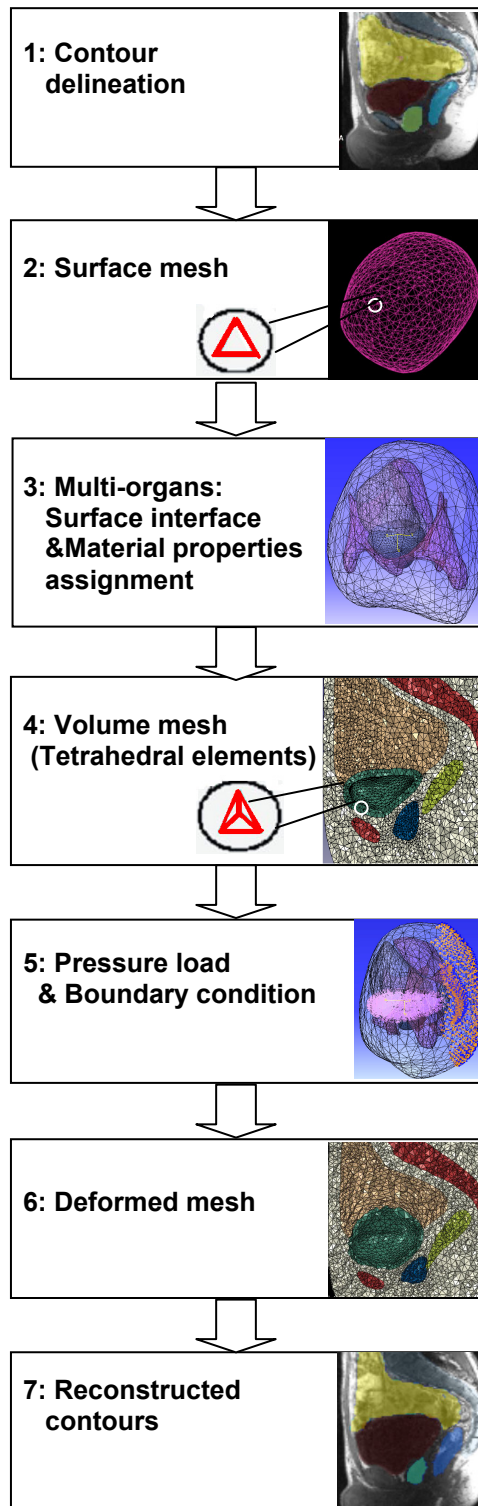


Figure 3.1: Flowchart of FEM construction and visualization procedure. (1) Contour delineation. (2) Surface mesh generation. (3) Creating surface interface between organs and assigning specific material properties to each organ. (4) Volume mesh generation. (5) Applying pressure load and boundary condition. (6) Organ deformation simulation. (7) Reconstruction of deformed organs.

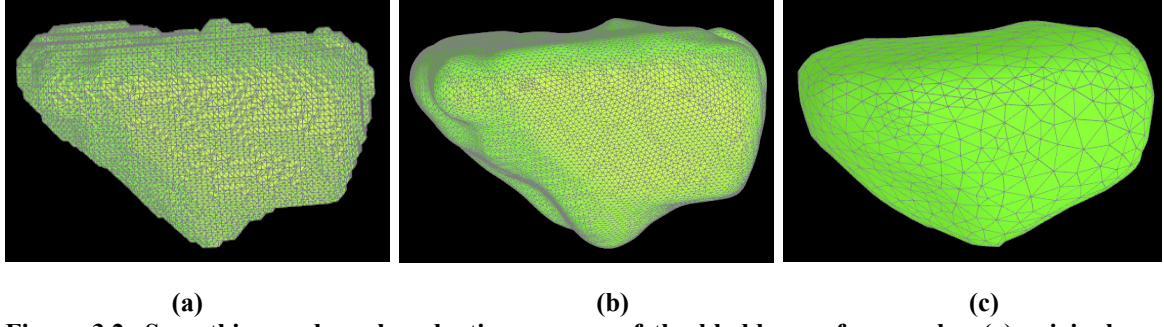


Figure 3.2: Smoothing and mesh reduction process of the bladder surface mesh : (a) original surface mesh generated by marching cubes algorithm, (b) results from (a) smoothed using a simple Laplacian smoothing operation with 5 iterations, (c) results from (b) whose surface triangulation number was reduced to 10% and smoothed with another 5 iterations.

3.2.4 FE Simulation and volume fitting

Once the load and boundary conditions were defined, finite element analysis (FEA) was performed to determine the displacements of all nodes in the model. A static direct single step was chosen for the FEA. The analysis was carried out on an Intel Duo Core CPU of 3.0 GHz with 8 GB of RAM and a 64 bits version of Windows XP. The average computation time for each model was 2 hours.

The result of FEA is a displacement vector of each volume node. Applying positive or negative scaling of these vectors allows construction of expanded or contracted bladders from the reference image. The scale factors were chosen such that the volume of the reconstructed bladder (enclosed by deformed outer bladder wall) was the same as the volume of the bladder in the test image. All images, including the reference, of each MR series were used as test images.

3.2.5 Accuracy and residual error calculation

We considered the bladder delineation on the test images as the ground truth, so we evaluated the accuracy of the bladder model by calculating the difference between the actual delineated bladder contours and the bladder contours predicted by the FEA.

We used the dice similarity coefficient (DSC) to measure the coincidence between the predicted and actual bladders. For two segmentations, R_1 and R_2 , the DSC was defined as the ratio of the volume of their intersection to their average volume:

$$DSC(R_1, R_2) = \frac{Volume(R_1 \cap R_2)}{\frac{1}{2}(Volume(R_1) + Volume(R_2))} \quad (3.3)$$

Note that the volumes of R_1 and R_2 were identical because of the volume fitting. The DSC has a value of 1 for perfect agreement and 0 when there is no overlap.

The surface mesh of the bladder in test images was resampled by 10, 000 randomly distributed surface nodes. The local residual error was defined by computing the

distance between each node on predicted bladder surface and its closest node in the resampled delineated bladder surface. The mean and standard deviation (SD) of the residual errors of all nodes were calculated for every bladder shape prediction.

3.3 Results

3.3.1 Scans

There were on average 6.3 (range, 4-8) MR scans acquired for the volunteers enrolled in this study. The average of bladder volume in all the series of scans was 405.9 ± 189.1 ml (1SD). The average bladder volume of all the reference images was 245.4 ± 30.1 ml (1SD).

3.3.2 Qualitative evaluation of the bladder model

The FE model was used to obtain insight in how the bladder deformation is affected by different resistance of surrounding structures. In a typical example (figure 3.3), we observed non-uniform expansion of the bladder wall, which occurred mainly in the cranio-anterior direction.

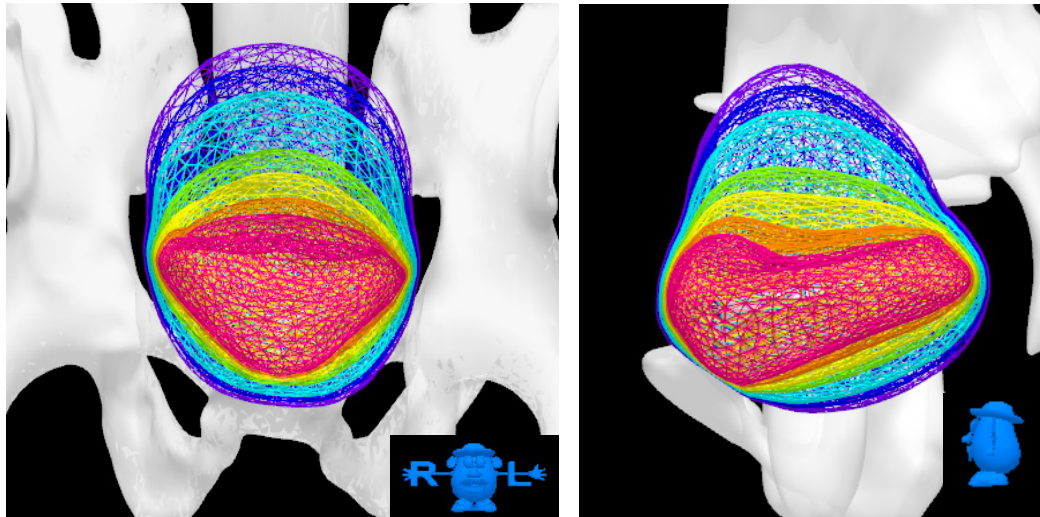


Figure 3.3: Results of bladder expansion simulation visualized in coronal and sagittal direction.

To verify the conformity of the bladder model, the predicted bladder surface was reconstructed and overlaid on the series of MR images, such as for example, for volunteer 1 (figure 3.4). Only small mismatches between the predicted and the real bladder surface occurred for bladder filling ratios between 50% and 200% of the reference volume (figure 3.4 a, b, d and e). However, the front part of the bladder showed larger discrepancies when the bladder filling increased beyond 200% of the original volume (figure 3.4 f, g and h).

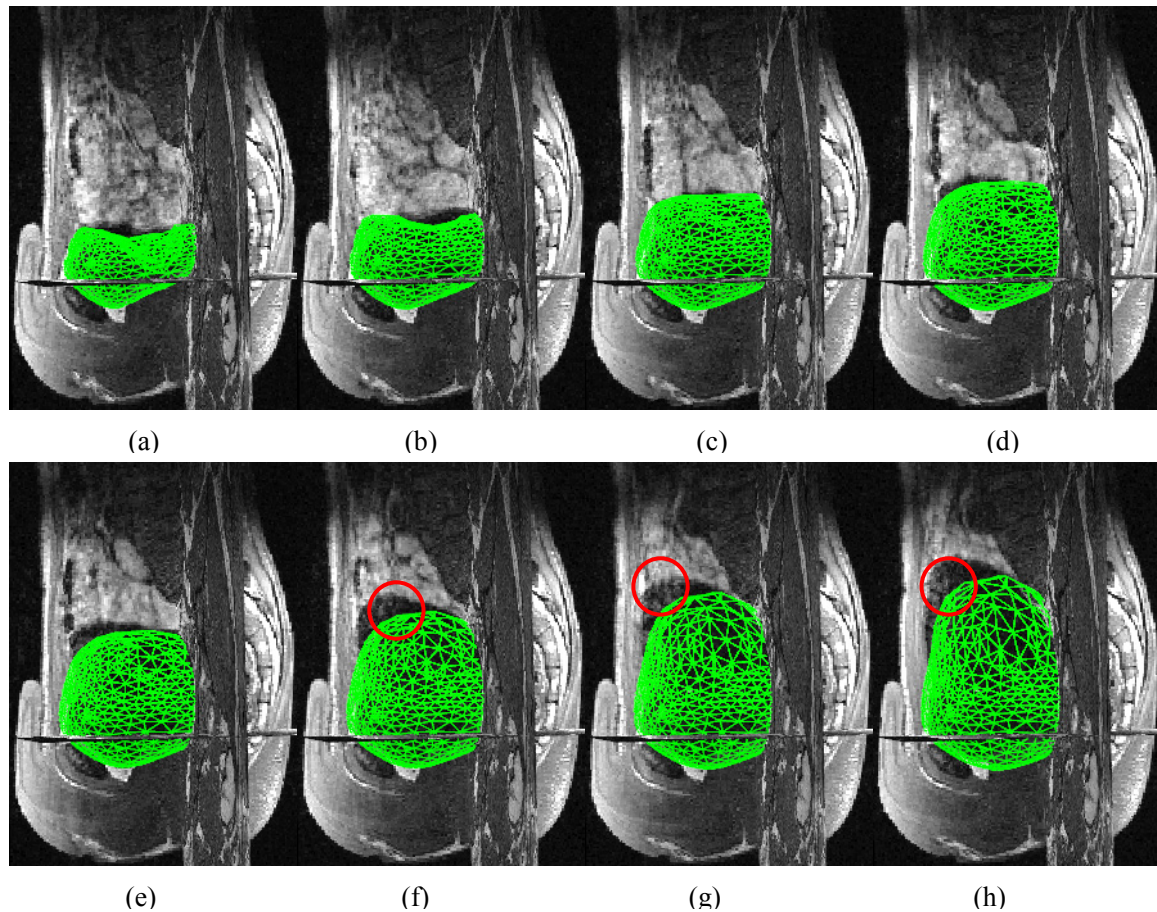


Figure 3.4: Predicted bladder surfaces (light green) overlaid on a series of MRI images, ordered from empty (a) to full bladder (h). (c) is the reference image, which, together with the volume change of the bladder, is the only input to the finite element model. The red circles indicate regions with discrepancies between the predicted bladder wall and actual bladder on the images.

Table 3.2: Mean of DSC, mean and SD of local residual error of the prediction model.

| Volunteer | Gender | Mean DSC | Local residual error | |
|----------------|--------|-------------|----------------------|-------------|
| | | | Mean (cm) | SD (cm) |
| 1 | male | 0.91 | 0.31 | 0.25 |
| 2 | male | 0.79 | 0.47 | 0.51 |
| 3 | male | 0.93 | 0.22 | 0.18 |
| 4 | male | 0.87 | 0.32 | 0.34 |
| 5 | male | 0.90 | 0.25 | 0.24 |
| 6 | female | 0.92 | 0.31 | 0.26 |
| 7 | female | 0.88 | 0.30 | 0.26 |
| 8 | female | 0.89 | 0.34 | 0.34 |
| 9 | female | 0.87 | 0.36 | 0.34 |
| 10 | female | 0.93 | 0.25 | 0.18 |
| Males | | 0.88 | 0.31 | 0.30 |
| Females | | 0.90 | 0.31 | 0.28 |
| All | | 0.89 | 0.31 | 0.29 |

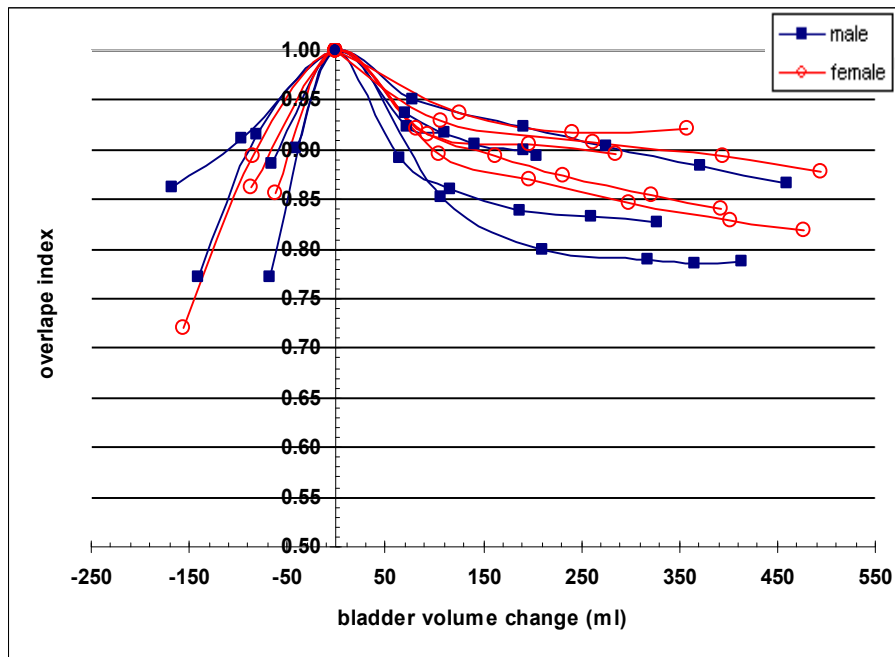


Figure 3.5: The overlap index between predicted and actual bladder contours versus bladder volume change for the ten volunteers. The icons and curves of male and female volunteers are labeled by blue square and red circle, respectively.

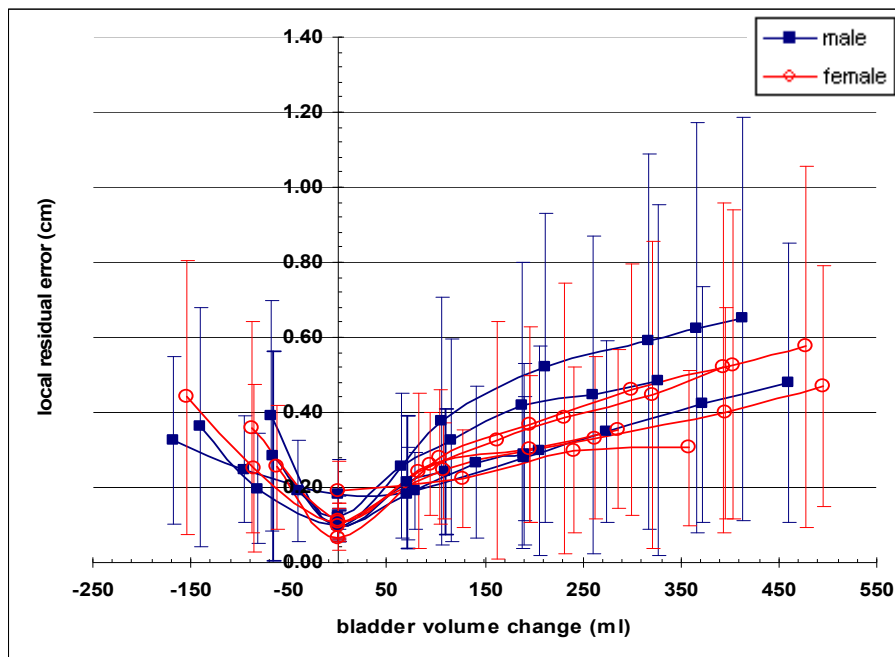


Figure 3.6: The mean and standard deviation (error bar) of local residual error between predicted and actual bladder surfaces versus the bladder volume change for the ten volunteers. The icons and curves of male and female volunteers are labeled by blue square and red circle, respectively.

3.3.3 Quantitative evaluation of bladder model

The mean DSC and mean and SD of the local residual errors for the bladder deformation prediction of 10 volunteers were presented in table 3.2. The mean DSC over 10 volunteers ranged from 0.78 to 0.93. There was no significant difference of the DSC between male and female groups ($p > 0.1$). The average DSC of all the test images was 0.89, and for each individual the DSC decreased with increasing bladder volume, as shown in figure 3.5. Pooling the data of the ten volunteers together, when bladder volume changed every 100 ml, the DSC value decreased by 0.05.

Figure 3.6 depicts the mean local residual errors related to the bladder volume change for each individual volunteer. The average mean and SD of local residual of all the volunteers were 0.31 cm and 0.29 cm. Within a range of 150 ml bladder volume change, the mean and SD were both smaller than 0.4 cm, however, the residual errors increased with the bladder volume increase. The largest error occurred in the volunteer 2. When bladder volume increased by 400 ml, the local residual errors reached 0.65 ± 0.54 cm (1SD). In figure 3.6 the residual error at 0 ml was not zero, which indicated a small systematic error of the local residual measure caused by the resampling of the surface vertices.

As an example, figure 3.7 visualizes the spatial distribution of the residual errors of volunteer 1 with a bladder volume increased by 200 ml. The largest residual errors occurred at the anterior and cranial part of bladder surface, i.e. at the place of the interface with small bowel. The residual errors calculated from the other test images showed similar distributions.

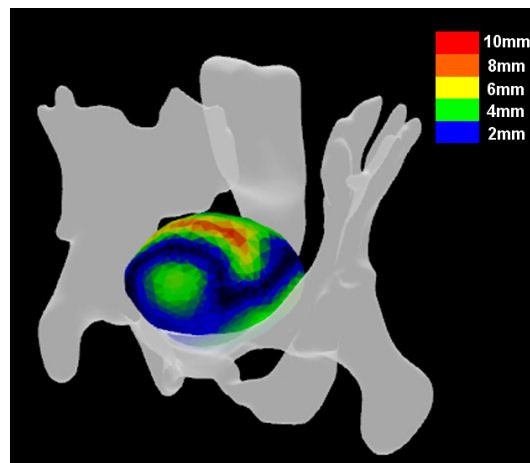


Figure 3.7: Color-coded projection of residual errors on bladder surface of volunteer 1 with the bladder volume increased by 200 ml.

3.4 Discussion

We presented an approach to construct a realistic 3D bladder model that simulates bladder deformation caused by bladder filling and predicts the short term bladder deformation using only bladder volume as input. Volume- and distance based measures were used to assess the accuracy of the bladder model. The agreement between simulation and real situation suggests that this FE bladder model is a feasible approach to predict the bladder deformation based on limited amount of observations.

Considering the FE simulation results, we observe that the increase of bladder volume does not only cause bladder wall deformations but also results in an interaction with all organs in the pelvis. The expansion of bladder inevitably leads to pushing the small bowel upwards, rotation of prostate in males or the deformation of uterus in females. In this simulation, we learned that in the pelvic region the small bowel and pelvic bone are the softest and stiffest structures, respectively, which determine the highly anisotropic deformation of bladder. This phenomenon should not be neglected when defining margins that ensure adequate dose coverage. It suggests the need for anisotropic margins for bladder cancer in whole bladder irradiation. The largest margin should be applied at the cranial side of the bladder next to the small bowel.

During about one hour, we did not find short-term bladder motion to be significantly affected by rectal or small bowel motion. This finding agrees with a previous study of short term bladder filling, in which the short-term rectal distention was found to be a much less important cause of bladder wall displacement than bladder filling [17;38].

The accuracy of the bladder model is highly correlated with magnitude of bladder volume change as shown in figure 3.6. Pinkawa et al. [77] reported the SD values of daily bladder volume are 124 ml with full bladder protocol and 56ml with empty bladder protocol. The bladder volume increase during a 28 min treatment time is 42 ± 47 ml [38]. In our study, the average SD of bladder volume in series of scans is 198.8 ml, which is larger than the inter- and intra-fraction bladder volume variations reported above. So, a higher accuracy could be achieved on patients with bladder cancer, especially for intra-fraction bladder motion prediction.

Compared with other bladder models [82;83], which describe the bladder deformation in a statistical way, our approach considers bladder filling change as a mechanical process and simulated the deformations caused by bladder filling change for the entire pelvis. This mechanical model showed some advantages. First, the model can be established based on just one scan, i.e. it needs much less prior information than statistical models. Second, the deformation of multiple organs can be calculated simultaneously, as the model is built for the entire pelvic region. Third, the results are described in terms of a vector field. Therefore, these data allow direct deformable dose accumulation for 4D planning of hollow and solid organs without interpolation.

However, the main drawback of the finite element modeling is that the accuracy is limited. The statistical bladder model [82] can reach fitting errors within 0.5 cm (0.2 cm on average), and the published PCA based method [83] models bladder deformation with residual error in the range of 0.15- 0.19 cm. The residual error of the finite element model (mean = 0.31 cm, SD = 0.29 cm, and local maximum error exceeded 1 cm) is larger than the errors in these two published statistical bladder

models. We expect that the poor definition of biomechanical material properties is the major limiting factor, as well as sliding of tissues that was not modeled. In this study a simplistic model, using population based linear elastic material properties was used, since complex patient-specific models are difficult to obtain for human tissues and non-linear model significantly increase computational time. However, in reality biological material always shows non-linear and non-elastic behavior [96-98]. Veronda et al. presented a material law which expresses the feature of soft tissue through an exponential term [96]. The most common nonlinear material models to describe the smooth muscle tissue are Odgen, Mooney-Rivlin and Yeoh models that are all available in Abaqus FE software [97;98]. In the future, such non-linear properties will be added to our model, as well as bladder tumors, which are known to be stiffer and deform less than the healthy part of the bladder wall [36]. Additionally material properties have been reported to be patient-specific [99;100], where the variation of the human tissue Young's modulus has been reported to be within $\pm 25\%$ of its mean values [99;101]. Especially for the small bowel and rectum, the bulk structures both include their content, probably causing the material properties of these two structures to vary largely between individuals and from day to day.

We did a limited material sensitivity analysis to test how the variation of elasticity between individuals affects the accuracy of the bladder model. For simplicity, 30% was considered as uncertainty of material parameters between individuals [101]. For volunteer one (illustrated in figure 3.4), the elasticity property Young's modulus of three important structures surrounding bladder, small bowel, body and prostate were increased and decreased 30% with reference value, respectively. We analyzed the effects of varying material parameters on the resulting bladder deformation. For the tested bladder volume increase of 200 ml, the bladder deformation prediction is not very sensitive to these changes. Given a 30% material uncertainty, only $<2\%$ change of overlap index and less than 0.5 mm change of mean and SD of local residual errors were observed (figure 3.8). This suggests that including more than one prior image to optimize patient-specific material properties can only slightly improve the accuracy of bladder model.

The new MR elastography technique might allow us to obtain more accurate material properties for every patient. This could result in a more accurate finite element model, utilizing actually measured material properties for every element [102;103].

Another limitation of this study is that the sliding between tissues in the deformation process was not included in the FE model. That is because of the poor definition of the friction factor in contact layers and a dramatic increase of computation time for this simulation.

An issue with the FE model is the long computation time. The whole process takes about 4 hours excluding the time required for organ delineating. It takes about 2 hours to construct the FE model, which needs user's intervention to make Boolean operations and mesh setting to assure the quality of mesh. The FE analysis with about 200, 000 nodes and 1, 200, 000 elements requires about 2 hours. We are currently investigating directly exporting the voxels in the image to the FE model as 8-node cubic element. The voxel-based mesh can be automatically generated from a binary image within two minutes. The computation efficiency and accuracy are comparable with the tetrahedral meshes that are used in this study. Since the voxel based mesh

generation approach can save about 2 hours' FE construction time and users' intervention, it makes the FE method more feasible and applicable to model bladder deformation in radiotherapy.

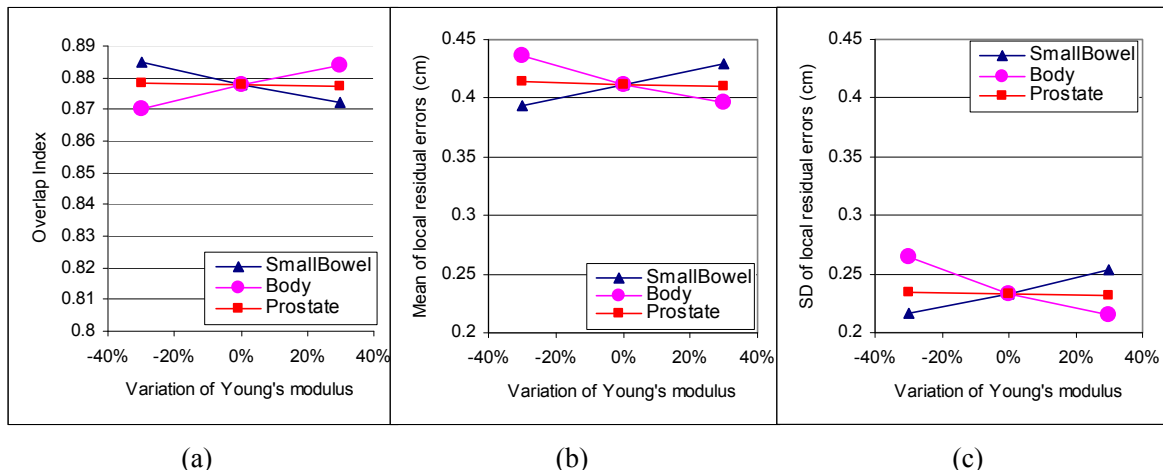


Figure 3.8: The accuracy of bladder deformation versus the uncertainty ($\pm 30\%$) in Young's modulus of structures of small bowel, body and prostate. (a), (b) and (c) show the overlap, mean and SD of the local residual errors between predicted and actual bladder surface of volunteer 1 with bladder volume increased by 200 ml, respectively.

3.5 Conclusion

We developed a 3D finite element model to simulate the interaction between pelvic organs solely caused by bladder volume changes. This model shows promise for the prediction of bladder deformation using just one image dataset and bladder volume changes as input. The accuracy levels achieved with this method are primarily limited by the inappropriate definition of material properties and sliding between organs, which has not been modeled. Such a bladder model gives insight into the interaction of pelvic organs and can potentially improve image-guided radiotherapy for bladder cancer patients, for example by predicting short-term movement.

Acknowledgements

The authors would like to thank Lambert Zijp (the Netherlands Cancer Institute) for the assistance with construction of the smoothed surface meshes. The authors are thankful to Hai Li and Zhenyu Wang (Beijing University of Aeronautics and Astronautics) and Yansheng Jiang (Leuven University) for the useful discussion about finite element method.